A Block Supramolecular Polymer and Its Kinetically Enhanced Stability

A block supramolecular polymer and its kinetically enhanced stability

Sung Ho Jung[1], Davide Bochicchio[2], Giovanni M. Pavan[2,*], Masayuki Takeuchi[1,*], Kazunori Sugiyasu[1,*]

[1]National Institute for Materials Science (NIMS), 1-2-1 Sengen, Tsukuba, Ibaraki 305-0047, Japan

[2]Department of Innovative Technologies, University of Applied Sciences and Arts of Southern Switzerland, CH-6928 Manno, Switzerland

E-mail: giovanni.pavan@supsi.ch (G.M.P.), TAKEUCHI.Masayuki@nims.go.jp (M.T.), SUGIYASU.Kazunori@nims.go.jp (K.S.)

Abstract

Biomolecular systems serve as an inspiration for the creation of multicomponent synthetic supramolecular systems that can be utilized to develop functional materials with unique properties. Nevertheless, supramolecular systems rapidly reach an equilibrium state through dynamic and reversible non-covalent bonds, resulting in a disorganized mixture of components rather than a system where each component functions cooperatively and/or independently. Therefore, efficient synthetic strategies and characterization methods for intricate multicomponent supramolecular assemblies need to be developed. Herein, we report the synthesis of supramolecular polymers (SPs) in which two distinct block segments are connected: i.e., block supramolecular polymers (BSPs). Previously reported crystallization-driven self-assembly approach was effective for this purpose. The obtained BSPs were endowed with enhanced stability depending on the block sequence. Furthermore, the block structure permitted the SP as an inner block to coexist with a reagent that was otherwise incompatible with the SP alone. These results are expected to pave the way for the design of more complex multicomponent supramolecular systems.

In the light of the substantial contribution of living polymerization to polymer science[1,2], the recent development of its supramolecular counterpart, i.e., living supramolecular polymerization[3,4], has inspired us to expand the scope of molecular self-assembly in the fields of materials science, nanotechnology, and biotechnology[5-7]. In this regard, the synthesis of block supramolecular polymers (BSPs), which offers unprecedented structural complexity and sophisticated functionality, has attracted considerable attention despite it being significantly challenging.

Based on the previous studies[8-21], we infer the prerequisites of living supramolecular polymerization and the issues associated with the synthesis of BSPs. First, the nucleation–elongation mechanism[22-25] should be operative so that supramolecular polymerization can be processed in a manner analogous to chain growth polymerization. In general, such supramolecular polymers (SPs) have high degrees of internal order (or crystallinity); accordingly, the synthesis of BSPs appears as difficult as welding two single crystals of different molecules. To this end, it is necessary to consider interfacial design between the two blocks, including intermolecular interactions and lattice matching[26]. Second, a metastable state has to be involved such

that an otherwise spontaneous nucleation process is kinetically suppressed. Formation of a competing aggregate[8,9] and intramonomer hydrogen-bonding[10-13,19,20] have been demonstrated to be effective for this purpose. However, it is still difficult to manage the pathway complexity because the delicate balance between the stabilities of the metastable species and SPs gets readily disrupted if the monomer structure is altered[9,12,27]. Given the abovementioned considerations, monomer design of the second block in a BSP is inevitably restricted by the monomer structure of the first block.

One-dimensional (1D) block nanostructures have been reported to date[28-36], and in particular, living crystallization-driven self-assembly (CDSA) has been demonstrated to be a powerful method to obtain such architectures via self-assembly[30-33]. Nevertheless, 1D block nanostructures with a *unimolecular* width (i.e., BSPs) are quite rare. Previously, van der Gucht, Otto, and co-workers[14] synthesized a BSP of peptide-based macrocyclic monomers bearing *benzyl* and *cyclohexylmethyl* side chains. We have also achieved a BSP of porphyrin monomers bearing *methoxy* (**2$_{Zn}$Me**) and *hexyloxy* (**2$_{Zn}$Hex**) side chains (Figure 1)[9]. These examples imply that monomer structures in BSPs have to be very similar, which corroborates the aforementioned

assertion. In fact, regarding our previous porphyrin systems, even a BSP consisting of different metal porphyrin cores (e.g., $\mathbf{2_{Zn}Me}$ and $\mathbf{2_{Cu}Me}$) could not be obtained (S. Ogi, M. Takeuchi, K. Sugiyasu, unpublished results). Accordingly, the functions and properties of BSPs arising from dissimilar SP blocks have thus far been virtually unexplored.

Herein, we assessed the applicability of the living CDSA method to the synthesis of unimolecular BSPs. In the living CDSA protocol, seeded-growth is performed by using both good and poor solvents for monomers. Recently, Manners and co-workers extended their living CDSA method to the supramolecular polymerization of platinum complexes and succeeded in controlling the length of SPs[15,16]. For the synthesis of BSPs, de Greef, Meijer, and co-worker[37] proposed a stepwise assembly of multicomponent structures by using good and poor solvents based on their in-depth mechanistic study; however, this strategy has not been attempted as yet.

We succeeded in connecting the SPs consisting of distinct porphyrin cores in B–A–B type triblock copolymer structures. Furthermore, it was found that the stability of block A could be kinetically enhanced by the presence of block B, which illustrates a

collective property of BSPs dictated by the block sequence. This study represents an important step toward the synthesis of advanced multicomponent SPs that have been increasingly attracting attention in recent years[38-43].

Results

Molecular design. As mentioned above, BSPs of different metal porphyrin monomers could not be obtained in our previous study (e.g., by using $\mathbf{2_{Zn}Me}$ and $\mathbf{2_{Cu}Me}$); instead, individual SPs were formed independently via a so-called self-sorting process[44-46]. We reasoned that these porphyrin cores are distorted differently[47] and prevent the dissimilar blocks from connecting to each other. To address this issue, we increased the number of hydrogen bonding sites so that the junction between the different metal porphyrin cores could be stabilized. The synthesis and characterization of the new monomers, namely, $\mathbf{4_{Zn}}$, $\mathbf{4_{Cu}}$, and $\mathbf{4_{2H}}$ (Figure 1), are described in the Supplementary Information.

Supramolecular polymerization. As discussed later, seeded-growth in living CDSA is typically performed in a mixed solvent system. In this study, a mixture of

methylcyclohexane (MCH): a poor solvent that induces self-assembly of porphyrin monomers, and toluene: a good solvent in which porphyrin monomers are molecularly dissolved, was used. Figure 2 illustrates the supramolecular polymerization of the zinc(II)-porphyrin monomer (**4$_{Zn}$**) in mixed solvents.

On increasing the proportion of MCH, the Soret band blue-shifted (Figure 2a,b), which suggested that the porphyrin chromophores were self-assembled in a face-to-face stacking manner, i.e., H aggregate mode[8,9]. Atomic force microscopy (AFM) visualized the 1D supramolecular polymer with a unimolecular height (Figure 2c). The plot of absorbance at 398 nm as a function of the proportion of MCH showed a critical MCH/toluene ratio as ~40% of MCH, at which complete disassembly occurs (Figure 2b). This result implied that supramolecular polymerization of **4$_{Zn}$** proceeded via the nucleation–elongation mechanism[37]. In fact, temperature-dependent absorption spectral changes (cooling process) accompanied a critical elongation temperature (T_e), a characteristic of the nucleation–elongation process (Figure 2d,f)[48-50]. We found a linear relationship between the T_e values and the proportion of MCH (Figure 2e).

Figure 2f compares the temperature-dependent degree of supramolecular

polymerization (α) obtained for solutions of different concentrations of $\mathbf{4_{Zn}}$; the results obtained for 67% MCH solution are shown as typical cooling curves. The elongation regime, i.e., the curve below T_e, could be fitted by the model developed by van der Shoot and Meijer[48]. The elongation enthalpy (h_e) determined from curve fitting was −108 kJ mol^{-1} for the curve of [$\mathbf{4_{Zn}}$] = 10 μM. The standard enthalpy ($\Delta H°$) and entropy ($\Delta S°$) for the elongation process were determined from a van't Hoff plot to be −119 kJ mol^{-1} and −271 J mol^{-1} K^{-1}, respectively (Figure 2g and Supplementary Figure 5). Thus, the Gibbs free energy ($\Delta G°$) at 298 K was calculated to be −38 kJ mol^{-1}. Likewise, supramolecular polymerization of $\mathbf{4_{Cu}}$ and $\mathbf{4_{2H}}$ was assessed, and the results are summarized in Table 1 (Supplementary Figures 7 and 8). AFM revealed that $\mathbf{4_{Cu}}$ and $\mathbf{4_{2H}}$ also formed 1D supramolecular polymers with a unimolecular width (Supplementary Figure 9).

As demonstrated above, the new porphyrin monomers ($\mathbf{4_{Zn}}$, $\mathbf{4_{Cu}}$, and $\mathbf{4_{2H}}$) have a strong propensity for supramolecular polymerization because of the increased number of hydrogen-bonding sites. Thus, it is anticipated that block junction between dissimilar SPs could be stabilized to produce BSPs. However, unlike our previous

system of $\mathbf{2_{Zn}Me}$[8,9], the supramolecular polymerization of these new monomers does not involve a metastable state, which eliminated the possibility of kinetic control over supramolecular polymerization (see the prerequisites discussed at the beginning of the article). As such, a dilemma was inherent in this monomer design, which led us to investigate whether living CDSA was applicable to the synthesis of unimolecular BSPs[15,16].

Living supramolecular polymerization. Figure 3a depicts the scheme of living supramolecular polymerization performed in the CDSA manner. Briefly, solutions of the seeds of a SP (in MCH) and a monomer (in toluene) were mixed to initiate the seeded-growth. As suggested by the plots of the temperatures at which the degree of supramolecular polymerization (α) reached 97% against the proportion of MCH, $\mathbf{4_{Zn}}$ is fully dissolved in toluene but self-assembles in MCH under ambient conditions ([$\mathbf{4_{Zn}}$] = 10 μM, Supplementary Figure 10). Provided a sufficiently high monomer concentration, this plot assures that a high α value (>95%) can be achieved when the solutions of the seeds (in MCH) and the monomer (in toluene) are mixed in a ratio of 2 to 1 at 298 K

(i.e., 67% MCH); this mixing ratio is used for the experiments that follow.

This scheme of living supramolecular polymerization requires seeds of a SP. By sonication (90 W at 2 °C for 3 h), SP**4**$_{\mathbf{Zn}}$ was fragmented into short pieces with the number average length (L_n) and weight average length (L_w) of 86 and 102 nm, respectively (Figure 3c). The absorption spectrum of these SP**4**$_{\mathbf{Zn}}$ seeds was identical to that of SP**4**$_{\mathbf{Zn}}$, indicating that the H aggregate mode was preserved (Supplementary Figure 11d).

The MCH solution of SP**4**$_{\mathbf{Zn}}$ seeds was placed carefully on the top of the toluene solution of monomeric **4**$_{\mathbf{Zn}}$ in a cuvette, which was then shaken for a few seconds at room temperature (Supplementary Figure 12). The color of the solution instantaneously changed to that of the H aggregate. The kinetics of the seeded-growth was too fast to be monitored even with the stopped-flow setup (not shown). The "depolymerization overshoot"[37] of the seed was not observed in both the manual mixing experiment and the stopped-flow experiment, although the proportion of the good solvent was suddenly increased.

Figures 3c and d show the AFM images of SP**4**$_{\mathbf{Zn}}$ obtained after

seeded-growth with different seed/monomer ratios (Supplementary Figure 13). The L_n and L_w increased in agreement with the feed ratio between the seed to the monomeric **4$_{Zn}$**. The polydispersity index (PDI, L_w/L_n) was as low as 1.20, indicative of controlled growth (Figure 3e). It should be noted that such a low PDI value could not be achieved without using the seed, i.e., if a toluene solution of **4$_{Zn}$** was mixed with pure MCH in the scheme shown in Figure 3a (Supplementary Figure 14). It is worth noting that the mixing processes (shaking, stirring, injection, etc.) also affected the PDI values, and it was necessary to optimize them as well; more specifically, rapid and homogeneous mixing of two solutions achieved lower PDI values. Further studies including the use of a variety of monomers with different structures and the combination of good/poor solvents are currently underway.

In the last decade, Manners and co-workers[30-33] have developed the living CDSA method and fabricated a variety of block nanostructures consisting of block copolymers. Fukushima, Aida, and co-workers[34] synthesized a linear heterojunction nanotubular object composed of small molecular entities (hexabenzocoronene derivatives). These seminal studies have demonstrated the unprecedented potential

applications of block nanostructures. Similarly, in the scheme shown in Figure 3a, other monomers such as $\mathbf{4_{Cu}}$ in its toluene solution could be used instead of $\mathbf{4_{Zn}}$. The increased L_n and low PDI values confirmed the controlled seeded-growth (Figure 3f,g,h and Supplementary Figure 15), thus suggesting the formation of a block supramolecular polymer, BSP($\mathbf{4_{Cu}}$-*b*-$\mathbf{4_{Zn}}$-*b*-$\mathbf{4_{Cu}}$). To the best of the authors' knowledge, this is the first example of a BSP with a unimolecular width composed of monomers based on distinct cores (not side chains[9,14]) that represents a new type of multicomponent SPs[38-43].

Kinetic stability of the block supramolecular polymers. The reversible nature of non-covalent bonds endows SPs with unique dynamic properties such as stimuli responsiveness and self-healing ability[5-7,51] However, it also leads to a drawback that SPs are inherently unstable, hindering their further applications to a certain extent. For example, SP$\mathbf{4_{Zn}}$ was readily depolymerized in the presence of Lewis bases that coordinated to the zinc atom and prevented the porphyrin plane from forming π-stacks. Upon the addition of 4-dimethylaminopyridine (DMAP), the H aggregate absorption

band of SP**4**$_{Zn}$ disappeared (398 nm) and a new band corresponding to DMAP-coordinated zinc(II)-porphyrin could be observed (430 nm) (Figure 4a). The Gibbs free energy for the coordination of DMAP to zinc(II)-porphyrin in the MCH/toluene (2/1) mixture was determined to be −29 kJ mol^{-1} at 298 K (Supplementary Figure 16), which rivaled the Gibbs free energy for the elongation of SP**4**$_{Zn}$ (−38 kJ mol^{-1}, see above). In contrast, SP**4**$_{Cu}$ was inert against DMAP because of the extremely low affinity of copper(II)-porphyrin for DMAP (Figure 4b)[52].

Interestingly, the depolymerization of SP**4**$_{Zn}$ by DMAP was prevented in the BSP(**4**$_{Cu}$-*b*-**4**$_{Zn}$-*b*-**4**$_{Cu}$) structure (Figure 4c,e and Supplementary Figure 17). This result implied that the SP**4**$_{Cu}$ blocks at both termini shielded the SP**4**$_{Zu}$ block and prevented it from DMAP-triggered depolymerization. For reference, the addition of DMAP to the mixture of SP**4**$_{Zn}$ and SP**4**$_{Cu}$ resulted in the depolymerization of SP**4**$_{Zn}$ only (Figure 4d). Heating the solution of BSP(**4**$_{Cu}$-*b*-**4**$_{Zn}$-*b*-**4**$_{Cu}$) above T_e in the presence of DMAP and subsequent cooling led to a solution with an absorption spectrum identical to that obtained for the reference mixture of SP**4**$_{Zn}$, SP**4**$_{Cu}$, and DMAP (compare red lines in Figure 4c and d). These results indicate that SP**4**$_{Zn}$ was kinetically stabilized against the

ligand in the block structure (Supplementary Figure 18). Previously, Meijer and co-workers[53,54] reported the synthesis of a random SP consisting of zinc(II)- and copper(II)-porphyrin monomers. These authors found that the zinc(II)-porphyrin monomer could be selectively removed from such a random SP by axial ligation with a Lewis base. A comparison of the kinetics of the system developed in the present study with Meijer's system may provide mechanistic insights into the depolymerization and exchange mechanisms.

Following previously reported methods for similar systems[55], molecular simulations was used in this study to obtain a molecular-level insight into these SPs and their DMAP-triggered depolymerization. All atom (AA) and coarse-grained (CG) models were developed for the $\mathbf{4_{Zn}}$ monomer (Figure 5a). The CG scheme employed in this work was consistent with that recently used for 1,3,5-benzenetricarboxamide (BTA)-based SPs, allowing us to study the SPs at a resolution of ~5 Å[56]. The AA model was used to fine-tune the CG model (see Method). A pre-stacked SP model of the initially extended CG $\mathbf{4_{Zn}}$ monomers was equilibrated in explicit cyclohexane solvent (equivalent to MCH at the level of resolution of these CG models) via CG molecular

dynamics (CG-MD) simulation[56,57]. An equilibrated configuration of SP**4**$_{Zn}$ was obtained, which appeared as a very stable, extended fiber of *unimolecular* width under these conditions (Figure 5b). Next, explicit CG DMAP molecules were inserted in the simulation box with a DMAP:**4**$_{Zn}$ ratio of 20:1, and the system was re-equilibrated. It was observed that the DMAP molecules were adsorbed onto the surface of SP**4**$_{Zn}$ without being able to access the zinc atoms in the interior of SP**4**$_{Zn}$. As shown in Figure 5c, it was only at the fiber tips that the DMAP molecules were stably coordinated to the porphyrin zinc atoms.

Next, the effect of DMAP on the depolymerization of SP**4**$_{Zn}$ was investigated. Following the recently reported method to study the dynamics of BTA-based SPs,[58] well-tempered metadynamics (WT-MetaD)[59] simulation was used to activate and explore the monomer exchange process (see Method). In the native condition (without DMAP), the global free energy difference between the assembled (**A**: N+1 assembled monomers) and disassembled state (**B**: N assembled + 1 disassembled) was found to be ~65 kJ mol^{-1} (Supplementary Figure 19). This value is in reasonable agreement with the experimentally determined ΔG for the elongation of SP**4**$_{Zn}$ in MCH (52 kJ mol^{-1},

Supplementary Figure 6). In the monomer exchange process from the SP**4**$_{\mathbf{Zn}}$ tips, the system had to overcome a free energy barrier of ~75 kJ mol^{-1} (Figure 5d, black). We also investigated monomer exchange process from the middle of SP**4**$_{\mathbf{Zn}}$ via WT-MetaD simulations. In this mechanism, the SP**4**$_{\mathbf{Zn}}$ first broke down to form a defect or a new tip (Step 1: ΔG_1 = ~70 kJ mol^{-1} needed), from which the monomer could then exchange (Step 2: see above): a mechanism also observed in BTA-based SPs in an organic solvent[58]. Assuming (underestimating) steps 1 and 2 as simply additive, and given the exponential relationship between the free energy barriers to cross and the characteristic probability for the events to occur, we can conclude that the monomer exchanges occurs predominantly from the fiber tips.

Interestingly, the same analysis on SP**4**$_{\mathbf{Zn}}$ in the presence of DMAP demonstrated that the free energy barrier for monomer exchange from the fiber tip decreased to ~40 kJ mol^{-1} (Figure 5d, red). Thus, free energy of the process was reduced by ~35 kJ mol^{-1} when compared to the same SP in the absence of DMAP, which was in agreement with the competing DMAP-zinc experimental affinity in MCH (~30 kJ mol^{-1}: see, Supplementary Figure 16). The free energy profile of monomer

dissociation from the fiber tip obtained from WT-MetaD under such out-of-equilibrium conditions demonstrated that the DMAP molecules interfered with the monomer–monomer interactions at the fiber tip, first by penetrating in between the porphyrin cores and then by facilitating monomer detachment from the fiber tip (Supplementary Figure 20). These results corroborate the stabilization scheme for BSPs demonstrated above, where SP**4**$_{Cu}$ blocks at both tips of the SP**4**$_{Zn}$ block could prevent SP**4**$_{Zn}$ from DMAP-triggered depolymerization, by saturating the *de facto* depolymerization "hot spots" (i.e., the SP**4**$_{Zn}$ tips).

Finally, to further explore the characteristics of the block structure, BSP(**4**$_{2H}$-*b*-**4**$_{Zn}$-*b*-**4**$_{2H}$) and BSP(**4**$_{Zn}$-*b*-**4**$_{2H}$-*b*-**4**$_{Zn}$) were synthesized following the above mentioned protocol and using the seeds of SP**4**$_{Zn}$ and SP**4**$_{2H}$, respectively ([**4**$_{Zn}$] = [**4**$_{2H}$] = 10 μM unless otherwise noted; Supplementary Figure 21, 22). Note that the supramolecular polymerization of **4**$_{2H}$ was probed by absorbance changes at 515 nm, which is the wavelength at which changes in the absorbance of **4**$_{Zn}$ were negligible (Figure 6a,b). Similarly, supramolecular polymerization of **4**$_{Zn}$ was selectively monitored at 541 nm. As demonstrated by the thermodynamic parameters (Table 1),

SP**4**$_{\mathbf{2H}}$ was thermally less stable than SP**4**$_{\mathbf{Zn}}$. More specifically, SP**4**$_{\mathbf{2H}}$ and SP**4**$_{\mathbf{Zn}}$ were characterized by T_e values of 306 and 326 K, respectively, as determined from their heating curves at the given concentration (Figure 6f,g). For a mixture of SP**4**$_{\mathbf{2H}}$ and SP**4**$_{\mathbf{Zn}}$, the two respective T_e values were observed independently (Figure 6c).

Although BSP(**4**$_{\mathbf{2H}}$-*b*-**4**$_{\mathbf{Zn}}$-*b*-**4**$_{\mathbf{2H}}$) and BSP(**4**$_{\mathbf{Zn}}$-*b*-**4**$_{\mathbf{2H}}$-*b*-**4**$_{\mathbf{Zn}}$) were spectroscopically indistinguishable (Figure 6d,e), their thermal depolymerization behaviors were quite different. BSP(**4**$_{\mathbf{2H}}$-*b*-**4**$_{\mathbf{Zn}}$-*b*-**4**$_{\mathbf{2H}}$) should depolymerize from the less stable SP**4**$_{\mathbf{2H}}$ block, and indeed the temperature-dependent changes in the absorbance of BSP(**4**$_{\mathbf{2H}}$-*b*-**4**$_{\mathbf{Zn}}$-*b*-**4**$_{\mathbf{2H}}$) were identical to that of the mixture of SP**4**$_{\mathbf{2H}}$ and SP**4**$_{\mathbf{Zn}}$ (Figure 6f,g). In stark contrast, BSP(**4**$_{\mathbf{Zn}}$-*b*-**4**$_{\mathbf{2H}}$-*b*-**4**$_{\mathbf{Zn}}$) was scarcely depolymerized even at 306 K, which is the T_e of SP**4**$_{\mathbf{2H}}$. The heating curve of BSP(**4**$_{\mathbf{Zn}}$-*b*-**4**$_{\mathbf{2H}}$-*b*-**4**$_{\mathbf{Zn}}$) observed at 515 nm resembled that of SP**4**$_{\mathbf{Zn}}$ observed at 550 nm.

To assess the kinetic stability, BSP(**4**$_{\mathbf{Zn}}$-*b*-**4**$_{\mathbf{2H}}$-*b*-**4**$_{\mathbf{Zn}}$) was kept at 308 K, which is a higher temperature than the T_e of SP**4**$_{\mathbf{2H}}$ (306 K), and the absorbance changes were monitored (Figure 6h,i). Although the absorbance of the SP**4**$_{\mathbf{Zn}}$ block (monitored at 541 nm, Figure 6i) was almost unchanged, the SP**4**$_{\mathbf{2H}}$ block (515 nm, Figure 6h) dissolved

over several tens of minutes. The rate of depolymerization of the SP$\mathbf{4_{2H}}$ block was linearly dependent on the concentration of $\mathbf{4_{Zn}}$ in the BSPs (Figure 6j). Thus, we infer that depolymerization of the SP$\mathbf{4_{2H}}$ block is controlled by the polymerization/depolymerization dynamics of the SP$\mathbf{4_{Zn}}$ block. Interestingly, the addition of DMAP accelerated the depolymerization of the SP$\mathbf{4_{2H}}$ block in the BSP($\mathbf{4_{Zn}}$-*b*-$\mathbf{4_{2H}}$-*b*-$\mathbf{4_{Zn}}$) (Figure 6h (iv)). These results demonstrated that the stability of the inner SP$\mathbf{4_{2H}}$ block was enhanced by the outer SP$\mathbf{4_{Zn}}$ block in the triblock copolymer sequence.

Discussion

The concept of living supramolecular polymerization has rapidly evolved in recent years[3,4,8-21]; nevertheless, the synthesis of BSPs still remains a challenge. As discussed at the beginning of this article, the dilemma of molecular design for connecting two distinct SPs needs to be addressed. Herein, it was demonstrated that BSPs could be synthesized via the living CDSA method[15,16,30-33]. Although the reaction conditions and mechanism of seeded growth remain to be explored from the viewpoint of kinetics, the

controlled length of the thus-obtained BSPs with narrow polydispersity confirmed that supramolecular polymerization occurred in the CDSA fashion. Furthermore, we found that BSPs have unique collective properties dictated by the block sequence.

It is noteworthy that SP$\mathbf{4_{Zn}}$, as an inner block in the BSP ($\mathbf{4_{Cu}}$-*b*-$\mathbf{4_{Zn}}$-*b*-$\mathbf{4_{Cu}}$), could coexist with DMAP that was otherwise incompatible with SP$\mathbf{4_{Zn}}$ alone. Thus, it appears that an SP can be *compartmentalized* in the block structure. As illustrated in many biomolecular systems, compartmentalization is a key concept for achieving intricate multicomponent systems; the present finding can lead to many opportunities for the design of unprecedented functional supramolecular systems. It would be worth noting that DMAP is not only a ligand but also a well-known organic catalyst. Obviously, an emergence of unique properties from the combination and sequence of the blocks can also be expected[60]. We believe that the synthetic strategy and characterization of BSPs demonstrated in this work will contribute to a better understanding of their attributes and applications for the development of multicomponent supramolecular systems.

References

1. Odian, G. Principles of polymerization, fourth edition (A John Wiley & Sons, Inc., Publication, Hoboken, New Jersey, 2004).

2. Lutz, J.-F., Lehn, J.-M., Meijer, E. W. & Matyjaszewski, K. From precision polymers to complex materials and systems. *Nat. Rev. Mater.* **1**, 1-14 (2016).

3. Vanderzwaag, D., DeGreef, T. F. A. & Meijer, E. W. Programmable supramolecular polymerizations. *Angew. Chem. Int. Ed.* **54**, 8334–8336 (2015).

4. Mukhopadhyay, R. D. & Ajayaghosh, A. Living supramolecular polymerization. *Science* **349**, 241–242 (2015).

5. Aida, T., Meijer, E. W. & Stupp, S. I. Functional supramolecular polymers. *Science* **335**, 813–817 (2012).

6. Webber, M. J., Appel, E. A., Meijer, E. W. & Langer, R. Supramolecular biomaterials. *Nat. Mater.* **15**, 13–26 (2015).

7. Yang, L., Tan, X., Wang, Z. & Zhang, X. Supramolecular polymers: historical development, preparation, characterization, and functions. *Chem. Rev.* **115**, 7196–7239 (2015).

8. Ogi, S., Sugiyasu, K., Manna, S., Samitsu, S. & Takeuchi, M. Living supramolecular polymerization realized through a biomimetic approach. *Nat. Chem.* **6**, 188–95 (2014).

9. Fukui, T. *et al.* Control over differentiation of a metastable supramolecular assembly in one and two dimensions. *Nat. Chem.* **9**, 493–499 (2017).

10. Kang, J. *et al.* A rational strategy for the realization of chain-growth supramolecular polymerization. *Science* **347**, 646–651 (2015).

11. Ogi, S., Stepanenko, V., Sugiyasu, K., Takeuchi, M. & Würthner, F. Mechanism of self-assembly process and seeded supramolecular polymerization of perylene bisimide organogelator. *J. Am. Chem. Soc.* **137**, 3300–3307 (2015).

12. Ogi, S., Stepanenko, V., Thein, J. & Würthner, F. Impact of alkyl spacer length on aggregation pathways in kinetically controlled supramolecular polymerization. *J. Am. Chem. Soc.* **138**, 670–678 (2016).

13. Wagner, W., Wehner, M., Stepanenko, V., Ogi, S. & Würthner, F. Living supramolecular polymerization of a perylene bisimide Dye into fluorescent J-aggregates. *Angew. Chem. Int. Ed.* **56**, 16008–16012 (2017).

14. Pal, A. *et al.* Controlling the structure and length of self-synthesizing supramolecular polymers through nucleated growth and disassembly. *Angew. Chem. Int. Ed.* **54**, 7852–7856 (2015).

15. Robinson, M. E. *et al.* Length control of supramolecular polymeric nanofibers based on stacked planar platinum(II) complexes by seeded-growth. *Chem. Commun.* **51**, 15921–15924 (2015).

16. Robinson, M. E. *et al.* Dimensional control and morphological transformations of supramolecular polymeric nanofibers based on cofacially-stacked planar amphiphilic platinum(II) complexes. *ACS Nano* **11**, 9162–9175 (2017).

17. Haedler, A. T. *et al.* Pathway complexity in the enantioselective self-assembly of functional carbonyl-bridged triarylamine trisamides. *J. Am. Chem. Soc.* **138**, 10539–10545 (2016).

18. Endo, M. *et al.* Photoregulated living supramolecular polymerization established by combining energy landscapes of photoisomerization and nucleation-elongation processes. *J. Am. Chem. Soc.* **138**, 14347–14353 (2016).

19. Ogi, S., Matsumoto, K. & Yamaguchi, S. Seeded polymerization through the

interplay of folding and aggregation of an amino-acid-based diamide. *Angew. Chem. Int. Ed.* 2339–2343 (2018).

20. Greciano, E. E., Matarranz, B. & Sanchez, L. Pathway complexity versus hierarchical self-assembly in N-annulated perylenes. Structural effects in seeded supramolecular polymerization. *Angew. Chem. Int. Ed.* doi:10.1002/anie.201801 (2018).

21. Mishra, A. *et al.* Biomimetic temporal self-assembly via fuel-driven controlled supramolecular polymerization. *Nat. Commun.* 9:1295 doi: 10.1038/s41467-018-03542-z (2018).

22. De Greef, F.A., Smulders, M.J., Wolffs, M., Schenning, A.P..H.J., Sijbesma, R.P., Meijers, E. W. Supramolecular polymerization. *Chem. Rev.* **109**, 5687–5754 (2009).

23. Zhao, D. & Moore, J. S. Nucleation-elongation: a mechanism for cooperative supramolecular polymerization. *Org. Biomol. Chem.* **1**, 3471–3491 (2003).

24. Chen, Z., Lohr, A., Saha-Möller, C. R. & Würthner, F. Self-assembled π-stacks of functional dyes in solution: structural and thermodynamic features. *Chem. Soc. Rev.* **38**, 564–584 (2009).

25. Rest, C., Kandanelli, R. & Fernández, G. Strategies to create hierarchical self-assembled structure *via* cooperative non-covalent interactions. *Chem. Soc. Rev.* **44**, 2543–2572 (2015).

26. Adolf, C. R. R., Ferlay, S., Kyritsakas, N. & Hosseini, M. W. Welding molecular crystals *J. Am. Chem. Soc.* **137**, 15390–15393 (2015).

27. Ogi, S., Fukui, T., Jue, M. L., Takeuchi, M. & Sugiyasu, K. Kinetic control over pathway complexity in supramolecular polymerization through modulating the energy landscape by rational molecular design. *Angew. Chem. Int. Ed.* **53**, 14363–14367 (2014).

28. Nicewarner-Pena, S. R. *et al.* Submicrometer metallic barcodes. *Science* **294**, 137–141 (2001).

29. Park, S., Lim, J.-H., Chung, S.-W. & Mirkin, C. A. Self-assembly of mesoscopic metal-polymer amphiphiles. *Science* **303**, 348–351 (2004).

30. Wang, X. *et al.* Cylindrical block copolymer micelles and co-micelles of controlled length and architecture. *Science* **644**, 644–648 (2007).

31. Gilroy, J. B. *et al.* Monodisperse cylindrical micelles by crystallization-driven living self-assembly. *Nat. Chem.* **2**, 566–570 (2010).

32. Rupar, P. A., Chabanne, L., Winnik, M. A. & Manners, I. Non-centrosymmetric cylindrical micelles by unidirectional growth. *Science* **337**, 559–562 (2012).

33. Hudson, Z. M., Lunn, D. J., Winnik, M. A. & Manners, I. Colour-tunable fluorescent multiblock micelles. *Nat. Commun.* 5:3372 doi: 10.1038/ncomms4372 (2014).

34. Zhang, W. *et al.* Supramolecular linear heterojunction composed of graphite-like semiconducting nanotubular segments. *Science* **334**, 340–343 (2011).

35. Beun, L. H., Albertazzi, L., van der Zwaag, D., de Vries, R. & Stuart, M. A. C. Unidirectional living growth of self-assembled protein nanofibrils revealed by suprer-resolution microscopy. *ASC Nano* **10**, 4973–4980 (2016).

36. Zhang, K., Yeung, M. C.-L., Leung, S. Y.-L. & Yam, V. W.-W. Living supramolecular polymerization achieved by collaborative assembly of platinum(II) complexes and block copolymers. *Proc. Natl. Acad. Sci.* **114,** 11844–11849 (2017).

37. Korevaar, P. A., Schaefer, C., de Greef, T. F. A. & Meijer, E. W. Controlling chemical self-assembly by solvent-dependent dynamics. *J. Am. Chem. Soc.* **134**, 13482–13491 (2012).

38. Besenius, P. Controlling supramolecular polymerization through multicomponent self-assembly. *J. Polym. Sci. A* **55**, 34-78 (2017).

39. Yagai, S. Supramolecularly engineered functional π-assemblies based on complementary hydrogen-bonding interactions. *Bull. Chem. Soc. Jpn.* 88, 28-58 (2014).

40. Görl, D., Zhang, X., Stepanenko, V. & Würthner, F. Supramolecular block copolymers by kinetically controlled co-self-assembly of planar and core-twisted perylene bisimides. *Nat. Commun.* 6:7009 doi: 10.1038/ncomms8009 (2015).

41. Hirao, T., Kudo, H., Amimoto, T. & Haino, T. Sequence-controlled supramolecular terpolymerization directed by specific molecular recognitions. *Nat. Commun.* 8:634 doi: 1038/s41467-017-00683-5 (2017).

42. Qin, B. *et al.* Supramolecular interfacial polymerization: a controllable method of fabricating supramolecular polymeric materials. *Angew. Chem. Int. Ed.* **56**, 7639–7643 (2017).

43. Miyauchi, M. & Harada, A. Construction of supramolecular polymers with alternating α-, β-cyclodextrin units using conformational change induced by competitive guest. *J. Am. Chem. Soc.* **126**, 11418–11419 (2004).

44. Safont-Sempere, M. M., Fernández, G. & Würthner, F. Self-sorting phenomena in complex supramolecular systems. *Chem. Rev.* **111**, 5784–5814 (2011).

45. van Esch, J. H. More than the sum of its parts. *Nature* **466**, 193–194 (2010).

46. Draper, E. R. & Adams, D. J. Low-molecular-weight-gels: the state of the art. *Chem* **3**, 390-410 (2017).

47. Valicsek, Z. & Horváth, O. Application of the electronic spectra of porphyrins for analytical purposes: The effects of metal ions and structural distortions. *Microchem. J.* **107,** 47–62 (2013).

48. Jonkheijm, P., van der Schoot, P., Schenning, A. P. H. J. & Meijer, E. W. Probing the solvent-assisted nucleation pathway in chemical self-assembly. *Science* **313**, 80–83 (2006).

49. Smulders, M. M. J., Schenning, A. P. H. J. & Meijer, E. W. Insight into the mechanisms of cooperative self-assembly: the 'sergeants-and-soldiers' principle of chiral and achiral C_3-symmetrical discotic triamides. *J. Am. Chem. Soc.* **130**, 606–611 (2008).

50. Smulders, M. M. J. *et al.* How to Distinguish isodesmic from cooperative supramolecular polymerisation. *Chem. Eur. J.* **16**, 362–367 (2010).

51. Torchi, A., Bochicchio, D. & Pavan, G. M. How the dynamics of a supramolecular polymer determines its dynamic adaptivity and stimuli-responsiveness: structure-dynamics-property relationships from coarse-grained simulations. *J. Phys. Chem. B* (2018). DOI: 10.1021/acs.jpcb.8b00428

52. Cremers, J. *et al.* Nanorings with copper(II) and zinc(II) centers: forcing copper porphyins to bind axial ligands in heterometallated oligomers. *Chem. Sci.* **7**, 6961–6968 (2016).

53. Helmich, F., Lee, C. C., Schenning, A. P. H. J. & Meijer, E. W. Chiral memory via chiral amplification and selective depolymerization of porphyrin aggregates. *J. Am. Chem. Soc.* **132**, 16753–16755 (2010).

54. Helmich, F., Smulders, M. M. J., Lee, C. C., Schenning, A. P. H. J. & Meijer, E. W. Effect of stereogenic centers on the self-sorting, depolymerization, and atropisomerization kinetics of porphyrin-based aggregates. *J. Am. Chem. Soc.* **133**, 12238–12246 (2011).

55. Bochicchio, D. & Pavan, G. M. Molecular modeling of supramolecular polymers. Adv. Phys. X **3**, 1436408 (2018).

56. Bochicchio, D. & Pavan, G. M. From cooperative self-assembly to water-soluble supramolecular polymers using coarse-grained simulations. *ACS Nano* **11**, 1000–1011 (2017).

57. Garzoni, M. *et al.* Effect of H-bonding on order amplification in the growth of a supramolecular polymer in water. *J. Am. Chem. Soc.* **138**, 13985–13995 (2016).

58. Bochicchio, D., Salvalaglio, M. & Pavan, G. M. Into the dynamics of a supramolecular polymer at submolecular resolution. *Nat. Commun.* 8:147 doi: 10.1038/s41467-017-00189-0 (2017).

59. Barducci, A., Bussi, G. & Parrinello, M. Well-tempered metadynamics: a smoothly converging and tunable free-energy method. *Phys. Rev. Lett.* **100**, 020603 (2008).

60. Schacher, F. H. Rupar, P. A. & Manners, I. Functional block copolymers: nanostructured materials with emerging applications. *Angew. Chem. Int. Ed.* **51**, 7898–7921 (2012).

Acknowledgements

This work was supported by KAKENHI (JP15H05483 for K.S.), Scientific Research on Innovative Arias “Dynamical ordering of biomolecular systems for creation of integrated functions (JP16H00787)”, “π-System figuration: control of electron and structural dynamism for innovative functions (JP26102009 for M.T.)”, and the Nanotechnology Network Project from the Ministry of Education, Culture, Sports, Science and Technology, Japan. S.H.J. thanks the Japan Society for the Promotion of

Science (JSPS) for a postdoctoral fellowship for overseas researchers (16F16043). D.B. and G.M.P. acknowledge the Swiss National Science Foundation (SNSF grant 200021_162827 to G.M.P.).

Author Contributions

S.H.J. and K.S. designed the experiments. S.H.J. performed all the experiments. D.B. and G.M.P. designed, performed, and analysed the simulations. S.H.J., G.M.P., and K.S. wrote the manuscript. All the authors discussed the results and commented on the manuscript.

Competing Interests Statement

The authors declare no competing financial interests.

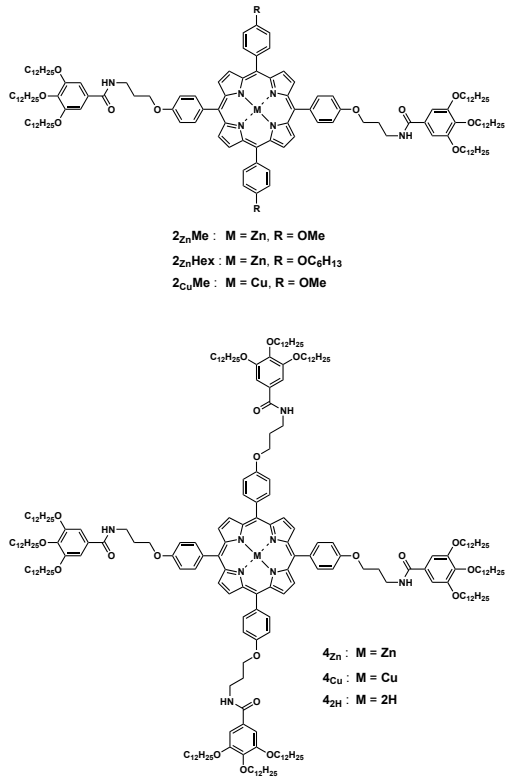

Figure 1. Structure of porphyrin-based monomers.

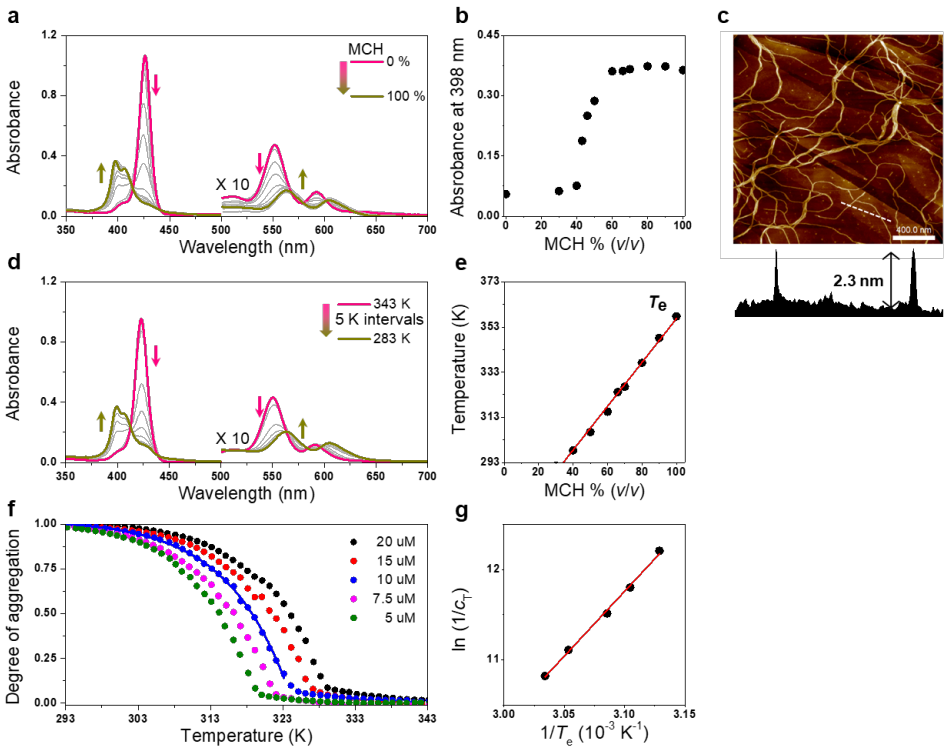

Figure 2. Supramolecular polymerization of a porphyrin-based monomer in MCH/toluene mixed solvent. (**a**) Absorption spectra of **4**$_{Zn}$ in MCH/toluene mixed solvents: [**4**$_{Zn}$] = 10 μM. (**b**) Plot of absorbance at 398 nm as a function of MCH proportion. (**c**) AFM image of supramolecular polymer of **4**$_{Zn}$ (i.e., SP**4**$_{Zn}$) prepared in MCH/toluene (2:1) mixed solvent: scale bar, 2 μm, and height profile of SP**4**$_{Zn}$ obtained across white lines in the AFM image. (**d**) Temperature-dependent absorption spectral changes of **4**$_{Zn}$ in MCH/toluene (2:1): [**4**$_{Zn}$] = 10 μM. (**e**) Plot of T_e values as a function of MCH proportion. (**f**) Changes in the degrees of supramolecular polymerization (α) as a function of temperature, with different concentrations of **4**$_{Zn}$ in MCH/toluene (2:1). A blue solid line is the fitting curve for [**4**$_{Zn}$] = 10 μM, obtained from cooperative model. (**g**) Plot of the natural logarithm of the reciprocal concentration at T_e ($c_{Mono}(T_e)^{-1}$) as a function of the reciprocal temperature (T^{-1}), showing a linear relationship (correlation coefficient of 0.998).

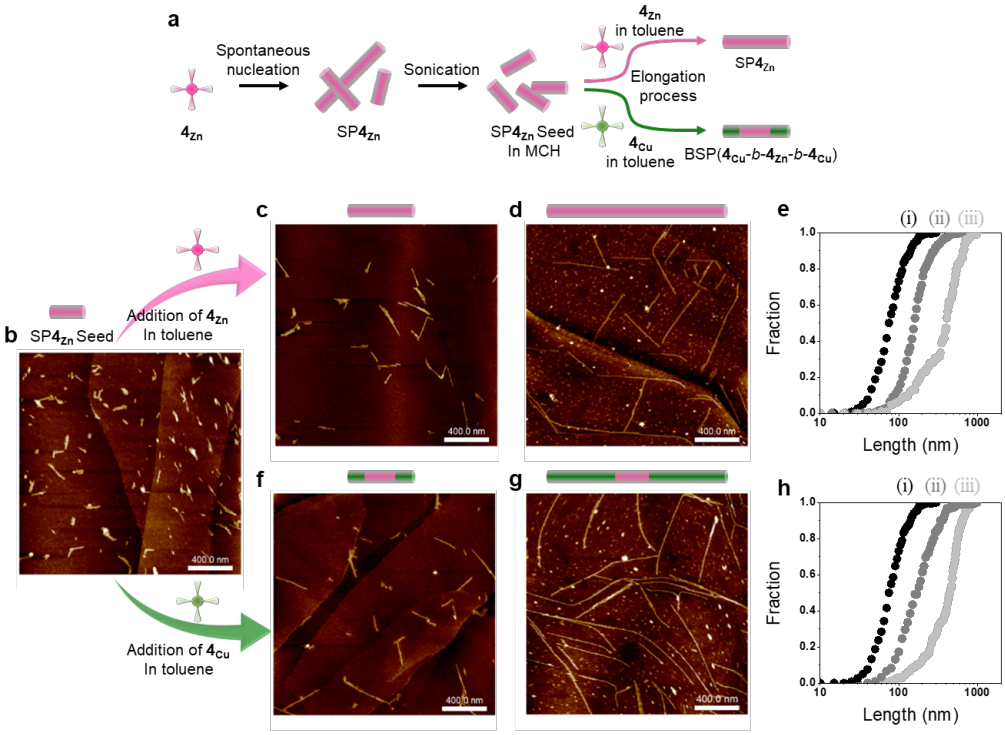

Figure 3. Living supramolecular polymerization and synthesis of block supramolecular polymers. (**a**) Schematic representation of living supramolecular polymerization performed via the CDSA method. (**b**) AFM image of seed of SP**4**$_{Zn}$: scale bar, 400 nm. (**c**,**d**) AFM images of SP**4**$_{Zn}$ prepared according to the scheme shown in (**a**): scale bar, 400 nm. The ratios between the seed of SP**4**$_{Zn}$ and monomeric **4**$_{Zn}$ are 1:1 (c) and 1:5 (d). (**e**) Cumulative histograms of the length distributions of the seed of (i) SP**4**$_{Zn}$ and SP**4**$_{Zn}$ prepared with the seed to monomeric **4**$_{Zn}$ ratios of (ii) 1:1 and (iii) 1:5. (**f**,**g**) AFM images of BSP(**4**$_{Cu}$-*b*-**4**$_{Zn}$-*b*-**4**$_{Cu}$) prepared according to the scheme shown in **a**, scale bar = 400 nm. The ratios of the seed of SP**4**$_{Zn}$ and monomeric **4**$_{Cu}$ were 1:1 (f) and 1:5 (g). (**h**) Cumulative histograms of the length distributions of the seed of (i) SP**4**$_{Zn}$ and BSP(**4**$_{Cu}$-*b*-**4**$_{Zn}$-*b*-**4**$_{Cu}$) prepared with the seed to monomeric **4**$_{Cu}$ ratios of (ii) 1:1 and (iii) 1:5.

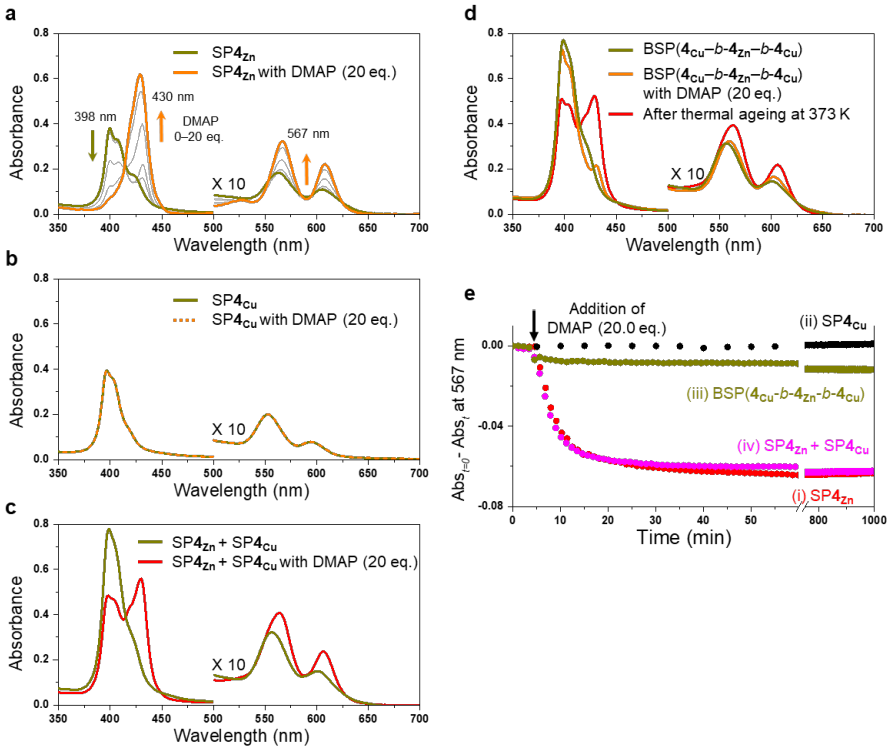

Figure 4. Kinetically enhanced stability of block supramolecular polymers. (**a**–**d**) Absorption spectra of SP**4**$_{Zn}$ (a), SP**4**$_{Cu}$ (b), a mixture of SP**4**$_{Zn}$ (c), and SP**4**$_{Cu}$ BSP(**4**$_{Cu}$-*b*-**4**$_{Zn}$-*b*-**4**$_{Cu}$) (d) with and without DMAP. (**e**) Time courses of absorbance changes because of the depolymerization of SP**4**$_{Zn}$ upon addition of DMAP: (i) SP**4**$_{Zn}$, (ii) SP**4**$_{Cu}$, (iii) a mixture of SP**4**$_{Zn}$ and SP**4**$_{Cu}$, and (iv) BSP(**4**$_{Cu}$-*b*-**4**$_{Zn}$-*b*-**4**$_{Cu}$).

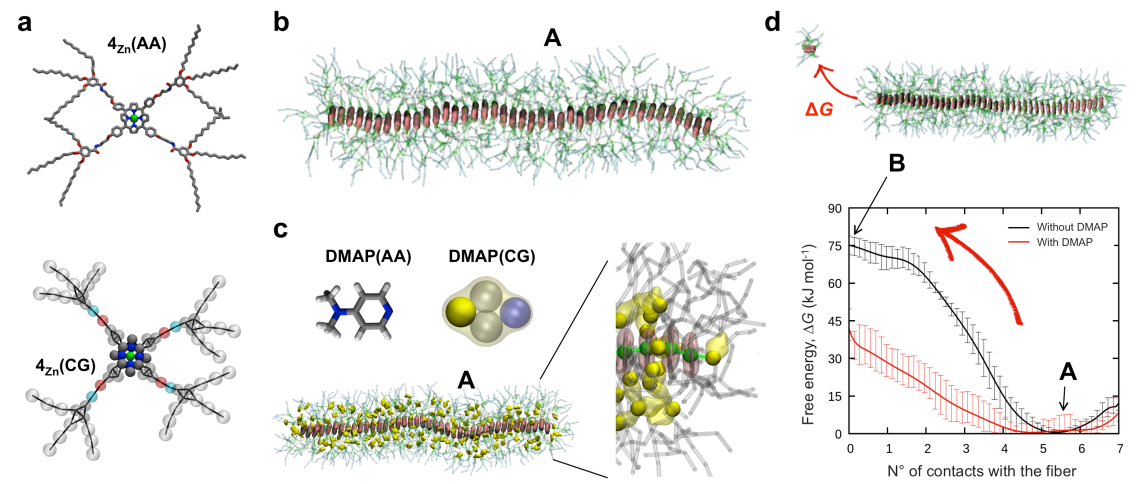

Figure 5. Molecular modeling of 4_{Zn} supramolecular polymer. (**a**) Atomistic (AA) and coarse-grained (CG) models for the $\mathbf{4_{Zn}}$ monomer. (**b**) Equilibrated configuration of the supramolecular fiber $\mathbf{4_{Zn}(CG)}$ in cyclohexane: zinc(II)-porphyrin cores are colored in pink and the side chains are represented as grey/green transparent wires (solvent not shown for clarity). (**c**) AA and CG models for DMAP. Equilibrated configuration of fiber $\mathbf{4_{Zn}(CG)}$ in cyclohexane (not shown) and DMAP (yellow). Only the DMAP molecules stably absorbed/interacting with the fiber are shown. Detail: DMAP coordination to zinc (in green); stable interactions are represented as green dynamic bonds. (**d**) Free energy (ΔG) for monomer exchange from the fiber tips (red arrow) obtained from WT-MetaD simulations. Data are shown as a function of the number of contacts between the exchanging monomer and the rest of the fiber (state A: assembled fiber; state B: exchange) for the $\mathbf{4_{Zn}(CG)}$ fiber in cyclohexane in the absence (black) and presence of DMAP (red).

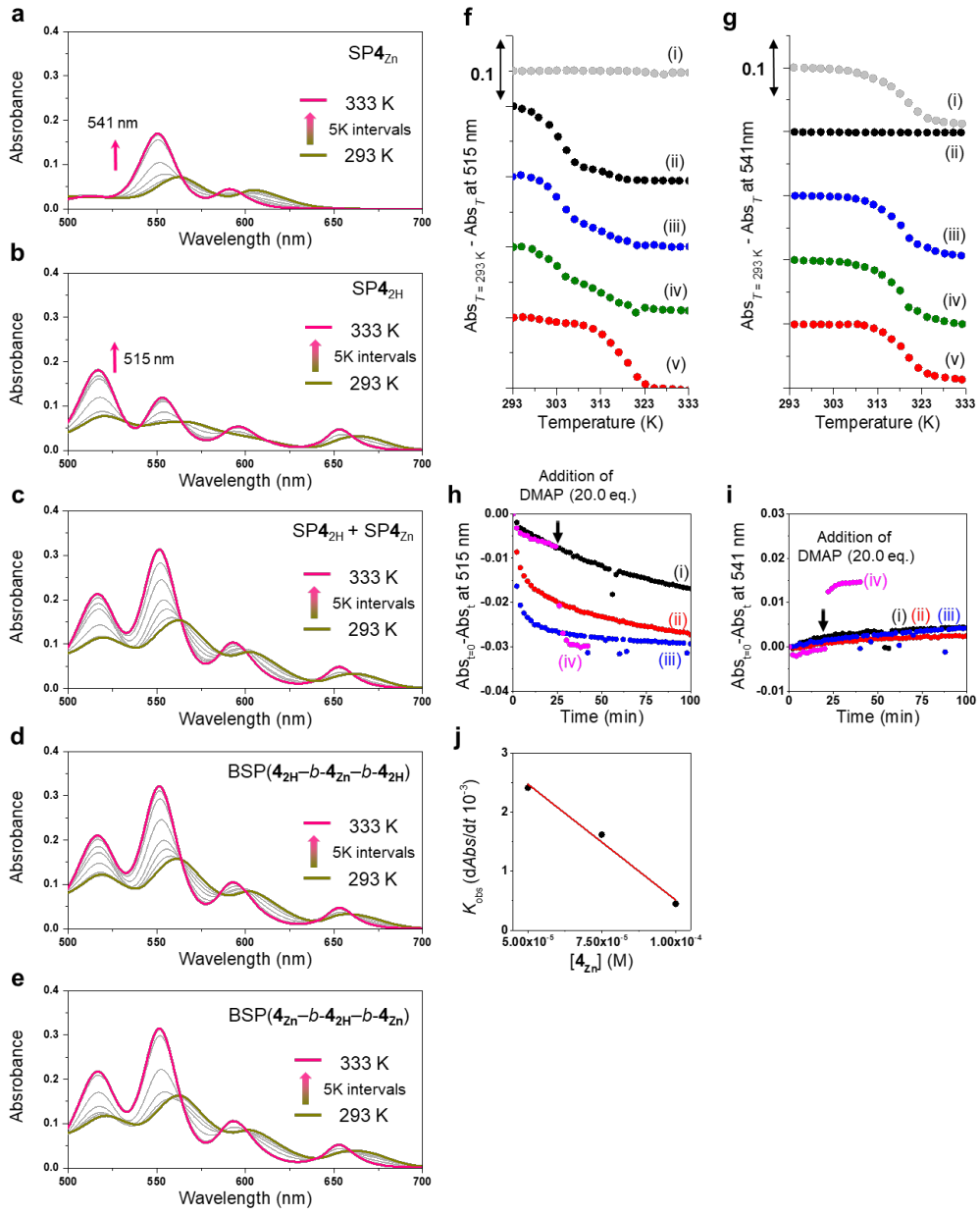

Figure 6. Kinetically enhanced stability of block supramolecular polymers. (**a**–**e**) Temperature-dependent absorption spectra of SP**4Zn** (a), SP**42H** (b), a mixture of SP**4Zn** and SP**42H** (c), BSP(**42H**-*b*-**4Zn**-*b*-**42H**) (d), and BSP(**4Zn**-*b*-**42H**-*b*-**4Zn**) (e). (**f**, **g**) Plots of absorbance at 515 nm (f) and 541 nm (g) as a function of temperature: (i) SP**4Zn**, (ii) SP**42H**, (iii) a mixture of SP**4Zn** and SP**42H**, (iv) BSP(**42H**-*b*-**4Zn**-*b*-**42H**), and (v) BSP(**4Zn**-*b*-**42H**-*b*-**4Zn**). (**h**, **i**) Time courses of absorbance changes at 515 nm (h) and 541 nm of BSP(**4Zn**-*b*-**42H**-*b*-**4Zn**) (i) at 308 K: [**42H**] = 10 μM, [**4Zn**] = 10 μM (i, iv), 7.5 μM (ii), and 5 μM (iii). In the case of (iv), DMAP (200 μM) was added after 20 min (see, arrow); the depolymerization of SP**42H** block was accelerated by the addition of DMAP (iv). (**j**) Plot of the depolymerization rate of SP**42H** block in BSP(**4Cu**-*b*-**4Zn**-*b*-**4Cu**) as a function of the concentration of **4Cu**.

Table 1. Thermodynamic parameters for supramolecular polymerization of porphyrin-based monomers in MCH and toluene mixture (2:1).

	T_e (at 10 μM) (K)	$\Delta H°$ (kJ mol^{-1})	$\Delta S°$ (J mol^{-1} K^{-1})	$\Delta G°$ (kJ mol^{-1})
4$_{Zn}$	324	−119	−271	−38
4$_{Cu}$	321	−122	−284	−37
4$_{2H}$	305	−128	−326	−31